THE JOURNAL OF BIOLOGICAL CHEMISTRY VOL. 291, NO. 35, pp. 18096–18106, August 26, 2016
© 2016 by The American Society for Biochemistry and Molecular Biology, Inc. Published in the U.S.A.

Structural and Biological Interaction of hsc-70 Protein with Phosphatidylserine in Endosomal Microautophagy*[S]

Received for publication, May 9, 2016, and in revised form, July 8, 2016 Published, JBC Papers in Press, July 12, 2016, DOI 10.1074/jbc.M116.736744

Kateryna Morozova[‡], Cristina C. Clement[‡], Susmita Kaushik[§], Barbara Stiller[§], Esperanza Arias[§], Atta Ahmad[¶], Jennifer N. Rauch[‖], Victor Chatterjee[‡], Chiara Melis[‡], Brian Scharf[‡], Jason E. Gestwicki[‖], Ana-Maria Cuervo[§], Erik R. P. Zuiderweg[¶1], and Laura Santambrogio[‡2]

From the Departments of [‡]Pathology and [§]Developmental Molecular Biology, Albert Einstein College of Medicine, New York, New York 10461, the [¶]Department of Biological Chemistry, University of Michigan Medical School, Ann Arbor, Michigan 48105, and the [‖]Department of Pharmaceutical Chemistry, University of California at San Francisco, San Francisco, California 94158

hsc-70 (HSPA8) is a cytosolic molecular chaperone, which plays a central role in cellular proteostasis, including quality control during protein refolding and regulation of protein degradation. hsc-70 is pivotal to the process of macroautophagy, chaperone-mediated autophagy, and endosomal microautophagy. The latter requires hsc-70 interaction with negatively charged phosphatidylserine (PS) at the endosomal limiting membrane. Herein, by combining plasmon resonance, NMR spectroscopy, and amino acid mutagenesis, we mapped the C terminus of the hsc-70 LID domain as the structural interface interacting with endosomal PS, and we estimated an hsc-70/PS equilibrium dissociation constant of 4.7 ± 0.1 μm. This interaction is specific and involves a total of 4–5 lysine residues. Plasmon resonance and NMR results were further experimentally validated by hsc-70 endosomal binding experiments and endosomal microautophagy assays. The discovery of this previously unknown contact surface for hsc-70 in this work elucidates the mechanism of hsc-70 PS/membrane interaction for cytosolic cargo internalization into endosomes.

hsc-70 (HSPA8) is a constitutively expressed molecular chaperone. The human hsp-70 chaperone family consists of 11 highly homologous members specific to different cellular compartments and organelles (1). hsc-70 resides in the cellular cytosol and nucleus and plays a central role in cellular proteostasis and protein trafficking.

Mammalian hsc-70 consists of the following four structural domains: a 44-kDa nucleotide binding domain (NBD)[3] (residues 1–384) with ATPase activity; a 12-kDa substrate binding domain (SBD) that binds to exposed hydrophobic sequences in client proteins (residues 385–505); a 10-kDa helical LID domain (residues 506–605); and a 5-kDa dynamically unstructured C-terminal domain (CTD) (residues 606–646) (2).

Binding of ATP in the NBD triggers a global conformational change that releases peptide/protein cargo from the SBD (3). Furthermore, hydrolysis of ATP closes the LID and greatly enhances client-SBD affinity (4). This hydrolysis cycle is important in the chaperone activity of hsc-70 as it allows, with the aid of different co-chaperones, iterative binding to clients resulting in protein (re)folding (5). Furthermore, hsc-70 is involved in recruitment of ubiquitin ligases (6), which leads to cargo polyubiquitination and subsequent hsc-70 trafficking to the proteasome or the endocytic pathway for cargo degradation (7).

Altogether, hsc-70's multiple interactions allow this chaperone to play an important role in several cellular activities, including ribosomal quality control, protein refolding, proteasome-linked degradation, macroautophagy, endosomal microautophagy, chaperone-mediated autophagy, endoplasmic reticulum/Golgi and mitochondrial targeting, and vesicle clathrin uncoating (8–17). These activities place hsc-70 as one of the master controllers of cellular proteostasis.

To carry out several of these functions, hsc-70 does not only interact with partner proteins but with membrane lipids as well (8, 16). Early on it was shown that incubation of hsc-70 with acidic phospholipid bilayers induces an ion conductance pathway (16). Subsequently, it was determined that, among all possible lipids, hsc-70 interacted with phosphatidylserine (PS) (16). Furthermore, our group determined that the hsc-70/PS interaction is pivotal for delivery of cytosolic cargo proteins to late endosomal compartments (8) in a process named endosomal microautophagy (eMI) and that electrostatic interactions between hsc-70 and PS were required for membrane binding (8).

Using a probe that monitors PS distribution in intact cells, Yeung *et al.* (17) determined that PS is present in the cytosolic leaflets of the plasma membrane, endosomes, and lysosomes and that an amphiphilic (cationic/hydrophobic) strategy is used by PS to recruit proteins (17). As such it was shown that PS-enriched endo-membranes recruit proteins with cationic

* This work was supported by National Institutes of Health Grants AG045223 (to L. S.), AG031782 (to A. M. C. and L. S.), NS059690 (to E. R. P. Z. and J. E. G.). The authors declare that they have no conflicts of interest with the contents of this article. The content is solely the responsibility of the authors and does not necessarily represent the official views of the National Institutes of Health.

[S] This article contains supplemental Figs. S1–S6.

[1] To whom correspondence may be addressed: Dept. of Biological Chemistry, University of Michigan Medical School, 1500 Medical Center Dr., Ann Arbor, MI 48105. E-mail: zuiderwe@umich.edu.

[2] To whom correspondence may be addressed: Dept. of Pathology, Albert Einstein College of Medicine, 1300 Morris Park Ave., New York, NY 10461. E-mail: laura.santambrogio@einstein.yu.edu.

[3] The abbreviations used are: NBD, nucleotide binding domain; PS, phosphatidylserine; SBD, substrate binding domain; CTD, substrate binding domain; DOPS, 1,2-dioleoyl-*sn*-glycero-3-phospho-L-serine; DOPC, 1,2-dioleoyl-*sn*-glycero-3-phosphocholine; BMP, bis-(monoacylglycero)phosphate; CSP, chemical shift perturbation; eMI, endosomal microautophagy; ANOVA, analysis of variance; PC, phosphatidylcholine; PDB, Protein Data Bank; LE, late endosome.

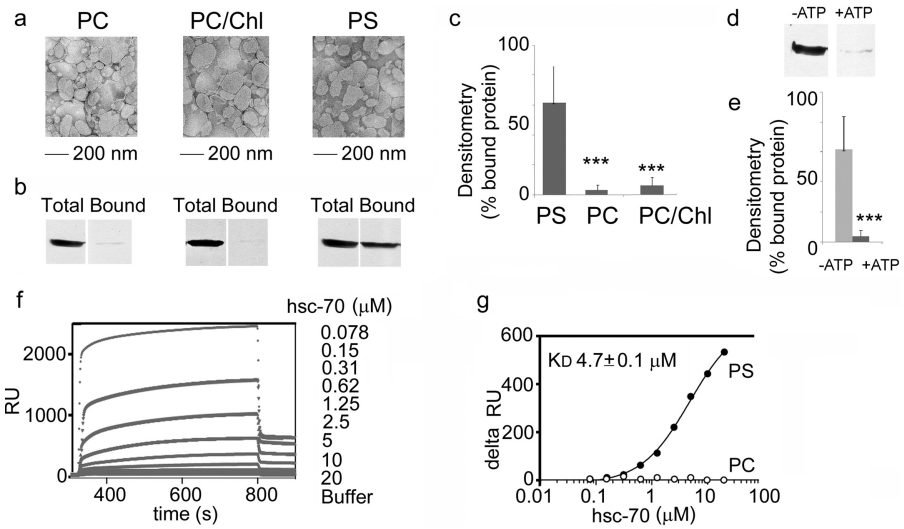

FIGURE 1. **C terminus of hsc-70 engage phosphatidylserine.** *a,* ultrastructural analysis of the extruded PS, PC, and PC/cholesterol (*PC/Chl*) liposomes used in the hsc-70 binding assays. *b,* Western blotting analysis of total hsc-70, as added in the liposome binding assay and the fraction bound to the liposomes. One of three experiments is shown. *c, bar graph* reporting the average and standard deviation of three experiments as detailed in *b*. Data were analyzed by one-way ANOVA (***, $p < 0.005$) and Tukey test. *d,* Western blotting analysis of liposome-bound hsc-70 in presence and absence of ATP. *e, bar graph* reporting the average and standard deviation of three experiments as detailed in *d*. Data were analyzed by one-way ANOVA (***, $p < 0.005$) and Tukey test. *f* and *g,* PS or PC lipid vesicles were immobilized on L1 BIAcore chips, and binding to hsc-70 was monitored. The results confirm that hsc-70 binds to PS but not PC. *RU*, response units.

charges, including members of the Ras and Rab families (17). By varying the surface charges of the membrane or the protein, the electrostatic interaction between PS and the target molecules could be modulated (17).

Even though it is recognized that membrane surface charges are fundamental for protein targeting, virtually nothing is known about the structural aspects or biophysics of these interactions. Here, we present a study combining biophysical methods (NMR spectroscopy and plasmon resonance) and mutagenesis to delineate the interaction between hsc-70 and PS. The results were validated with endosomal transport assays determining the role of the hsc-70/PS interaction on endosomal microautophagy. We conclude that positively charged residues at the C terminus of the hsc-70 LID domain are interacting most strongly with the negatively charged phosphatidylserine. This interaction is surprisingly specific and involves a few lysine residues. The discovery of this previously unknown contact surface for hsc-70 in this work elucidates the mechanism of hsc-70 PS/membrane interaction for cytosolic cargo internalization into endosomes.

Results

hsc-70 Engages Phosphatidylserine—We previously reported that hsc-70 binding to PS is required for protein internalization from the cytosol to endosomal compartments for their degradation through what is now termed eMI (8). To further characterize this interaction, liposomes composed of phosphatidylcholine (PC), PC/cholesterol, or PS were incubated with full-length hsc-70 (Fig. 1*a*). Following incubation for 30 min, liposomes were pelleted by ultracentrifugation to determine the amount of liposome-bound hsc-70. As reported previously (8), Western blotting analysis confirmed that hsc-70 only binds to PS/liposome but not to PC or to PC/cholesterol liposomes (Fig. 1, *a*--*c*). Additionally, the PS-hsc-70 binding was inhibited by the presence of ATP (Fig. 1, *d* and *e*). To confirm binding of hsc-70 to PS and to quantify the affinity, we immobilized extruded lipid vesicles on L1 BIAcore Chips and measured binding to hsc-70 by surface plasmon resonance. Consistent with the other binding platforms, hsc-70 bound to PS ($K_D = 4.7 \pm 0.1$ μM) but did not bind to PC ($K_D > 20$ μM) (Fig. 1, *f* and *g*).

Interaction of hsc-70/SBD with PS as Visualized by NMR—We used NMR spectroscopy to map the interaction of PS on the human hsc-70 substrate binding domain (residues 395–605). This construct contains both the β-basket (residues 395–503) with the hydrophobic substrate binding cleft as well as the putative complete α-helical lid (residues 504–605) (Fig. 2). The terminology "putative" is used because to date there is no complete three-dimensional structure available for these domains of hsc-70.

All NMR experiments were carried out with ^{15}N-labeled SBD, using TROSY-HSQC. The first experiments monitored hsc-70 chemical shift perturbations (CSP) upon addition of 1,2-dioleoyl-*sn*-glycero-3-phospho-L-serine (DOPS) directly dissolved in the experimental buffer. The CSPs were small but distinct (Fig. 2*a* and supplemental Fig. S1). A histogram of CSPs is shown in Fig. 2*b*, and the most significant of these shifts are color-coded on a homology model in supplemental Fig. S2. Clearly, NH shifts of many residues are affected by DOPS. This is not unexpected because many positively charged residues could potentially interact with the negatively charged DOPS. In fact, it would not be unreasonable to anticipate that every positive residue in the protein would be about equally affected by the presence of DOPS if no specific interaction took place. However, that was not the case. Lysines and arginines in the last 40 residues of the LID domain were significantly more perturbed than others (Fig. 2*c*) indicating a limited and specific interaction area. The most significant

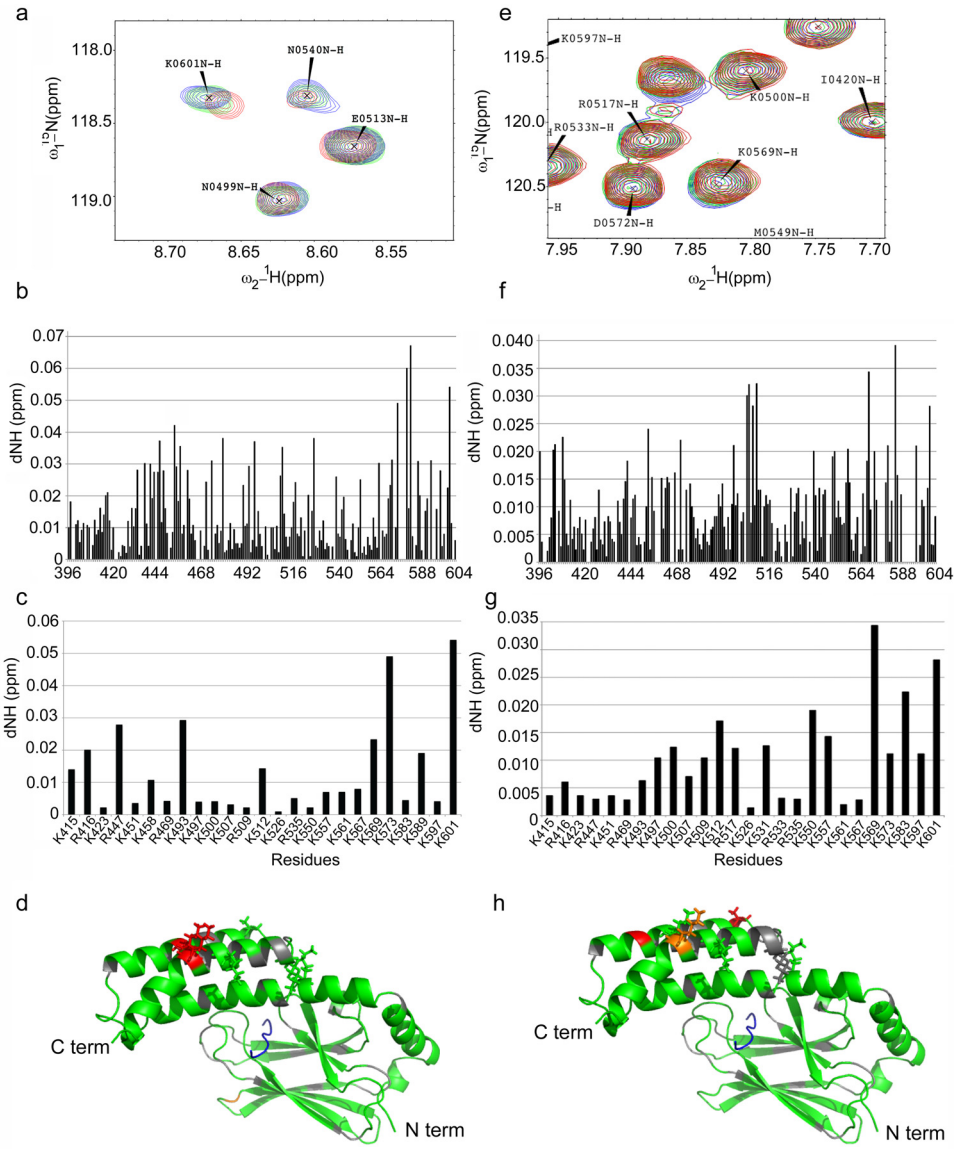

FIGURE 2. **NMR studies of the interaction of hsc-70 SBD with DOPS.** *a,* overlay of two-dimensional ^{15}N-^{1}H TROSY-HSQC spectra of 45 mM hsc-70(395–604) without (*blue*) and with (*green*) 160 mM and 1600 μM DOPS (*red*). The figure is an enlargement highlighting the DOPS-induced chemical shift perturbation of Lys-601. *b,* amide group chemical shift perturbations (dNH = $\sqrt{(\Delta\delta N^2 = \Delta\delta H^2)}$ δ) resulting from adding 1.65 mM DOPS to 45 mM hsc-70 SBD in the presence of 165 mM hydrophobic TAU peptide KVQIINKKGCGMGHHHHHH blocking the substrate-binding cleft. *c,* lysine and arginine residue amide group chemical shift perturbations resulting from adding 1.65 mM DOPS to 45 mM hsc-70 SBD in the presence of 165 mM of the hydrophobic TAU peptide. *d,* homology model of hsc-70 SBD based on the crystal structure of hsp-70 SBD complexed with NRLLLTG (PDB code 4PO2). The figure is color-coded for the NH chemical shift perturbations resulting from adding 1.65 mM DOPS to 45 mM hsc-70 SBD in the presence of 165 mM hydrophobic TAU peptide. Only shifts for Lys and Arg NH are shown. In *green* are NH shifts smaller than two S.D.; in *orange* are 2 S.D. < CSP < 3 S.D., and in *red* CSP > 3 S.D. *Gray* indicates unassigned/overlapped. Residues Arg-535, Lys-573, Lys-583, Lys-589, Lys-597, and Lys-601 for which mutagenesis studies were carried out are rendered as *sticks*. The backbone of the bound NRLLLTG is shown in *blue*. *e,* overlay of two-dimensional ^{15}N-^{1}H TROSY-HSQC spectra hsc-70(395–604) without (*blue*, hsc 80 mM) and with sub-equivalent DOPS nano-discs (*green*, hsc 57 mM, discs 36 mM), and supra-equivalent DOPS nano-discs (*red*, hsc 44 mM, discs 55 mM). The figure is an enlargement highlighting the DOPS-induced chemical shift perturbation of Lys-569. *f,* amide group chemical shift perturbations resulting from adding 55 μM DOPS nano-discs to 44 μM hsc-70 SBD in the presence of 50 μM hydrophobic peptide MHHHHHHSSGVDLGTENLYFQ blocking the substrate-binding cleft. *g,* lysine and arginine residue amide group chemical shift perturbations resulting from adding 55 mM DOPS nano-discs to 44 mM hsc-70 SBD in the presence of 50 mM hydrophobic peptide. *h,* homology model of hsc-70 SBD. The figure is color-coded for the NH chemical shift perturbations resulting from adding 55 mM DOPS nano-discs to 44 mM hsc-70 SBD in the presence of 50 mM hydrophobic peptide. Only shifts for Lys and Arg NH are shown. In *green* are NH shifts smaller than 2 S.D.; in *orange* 2 S.D. < CSP < 3 S.D., in *red* CSP > 3 S.D. *Gray* indicates unassigned/overlapped. Residues Arg-535, Lys-573, Lys-583, Lys-589, Lys-597, and Lys-601 for which mutagenesis studies were carried out are rendered as *sticks*. The backbone of the bound NRLLLTG is shown in *blue*.

of these shifts are color-coded on the homology model in Fig. 2*d*.

At the conditions used, between 33 and 1650 μM DOPS, the phospholipid (with critical micellar concentration <1 μM) should form large vesicles (as large as 1000 Å). If hsc-70 were to form a rigid complex with such entities, its NMR spectrum would become undetectable (because NMR line width is proportional to molecular weight). However, the recorded spectra (Fig. 2*a* and supplemental Fig. S1) show little or no line broadening even in the presence of a large excess of DOPS. This result suggests two possibilities, either the hsc-70 LID domain is loosely tethered to the fluid-like vesicle surface or the observed hsc-70 interaction is with smaller entities such as micelles or individual lipid molecules.

To distinguish between these possibilities, we carried out a second series of experiments, this time using DOPS molecules encapsulated in nano-discs (18). These discs contain a bi-layer of phospholipids, have a uniform molecular size of 100 Å, and are restrained by protein oligomer that acts like a molecular belt. We were attracted to the use of nano-discs because they are so stable that they could be purified by gel filtration to remove free lipid, micelles, and proteins (18).

NMR titrations with the purified DOPS nano-discs were carried out at lower molecular ratios (55 μM DOPS nano-discs and 44 μM hsc-70) to enhance specificity. The results were similar to those obtained with the DOPS vesicles, demonstrating that the CSPs in either set of experiments are not due to interaction with free lipids or micelles, but with the surface of large molecular entities. Again, no line broadening could be observed (Fig. 2*e* and supplemental Fig. S3). Specifically, with a K_D of 5 μM, the 44 μM hsc-70 in the presence of 55 μM DOPS nano-discs should be bound 80% of the time. At the outset, one should therefore expect that the protein acquires 80% of the hydrodynamic properties of the large particle, which would result in excessive line broadening. As it does not, this must indicate that the hsc-70 LID domain is loosely tethered to the fluid-like nano-disc surface while bound. The situation is reminiscent of the delocalized interaction of DnaJ J-domain to DnaK (the Hsp70 of *Escherichia coli*) (19), cytochrome-cytochrome complexes (20), and nonspecific protein/DNA interactions (21), all of which are, like the hsc70/PS interaction, electrostatic in nature.

Similar to the vesicle interaction, the NH shifts of many hsc-70 residues are affected by the DOPS nano-discs (Fig. 2*f* and supplemental Fig. S4). But even more clearly, it is seen that lysines and arginines in the last 40 residues of the LID domain are perturbed more than other basic residues in the protein (Fig. 2*g*). The most significant of these shifts are color-coded on the homology model (Fig. 2*h*). No significant changes could be discerned in the NMR spectra hsc-70 NBD(1–386) upon addition of DOPS vesicles (results not shown), indicating specificity for the SBD-LID domain.

Together, the NMR experiments strongly indicate that positively charged residues at the C terminus of the hsc-70 LID domain are interacting most strongly with the negatively charged DOPS phospholipids. The interaction is surprisingly specific and involves only a few lysine residues. The PS-binding area has not previously been identified as an intermolecular interface of hsc-70.

Phosphatidylserine Binding of hsc-70 Mutants—To validate that the amino acids mapped by NMR are involved in the hsc-70/PS interactions, the following mutants were generated: R533A, K535A, K573Q, K583Q, K589Q, K597Q, and K601Q. Circular dichroism was employed to analyze each mutant's secondary structure as compared with wild type, ensuring that the mutation did not alter the hsc-70 folding. As presented in Fig. 3*a*, the CD spectra of the hsc-70 mutants overlapped with the one for the hsc-70 wild type. One interesting mutant, notably K569Q, could not be generated because the mutated protein increased its tendency to aggregate and lose its secondary structure.

Liposome binding assay was performed, as described above, with PS-based liposomes to validate the hsc-70/PS interaction

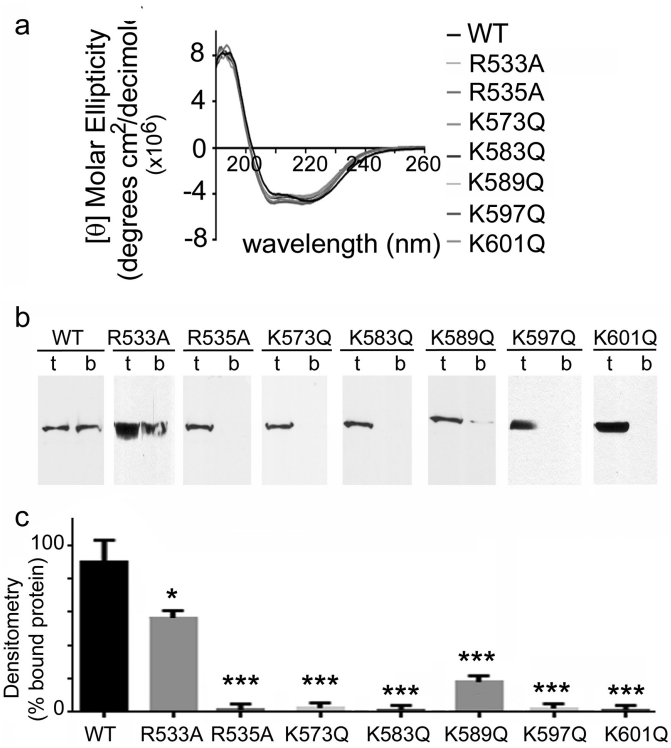

FIGURE 3. **Phosphatidylserine binding of hsc-70 mutants.** *a,* circular dichroism to validate correct folding (secondary and tertiary structures) of hsc-70 mutants (R533A, K535A, K573Q, K583Q, K589Q, K597Q, and K601Q) as compared with wild-type hsc-70. *b,* Western blotting analysis of total wild-type and mutants hsc-70, as added in the liposome binding assay, and the fraction bound to the liposomes are shown. *t*, total; *b*, bound. *c,* mean and standard deviation of four different liposome-binding experiments, as reported in *b*. Data were analyzed by one-way ANOVA (*, $p < 0.05$; ***, $p < 0.005$) and Tukey test.

sites, as mapped previously by NMR. A statistically significant decrease in PS binding of different extents could be observed for each mutant, as compared with wild-type hsc-70 (Fig. 3, *b* and *c*). Altogether, the liposome binding assay confirmed the relevance of the lysines and arginines in the C-terminal LID region of hsc-70 for PS interaction.

Biological Role of the hsc-70-PS Complex in Cytosol-to-Endosome Protein Internalization—We previously demonstrated that hsc-70/PS interaction is required for internalization of cytosolic proteins in late endosomal compartments through ESCRT-mediated microvesicles that form in the endosomal surface (8). This process, also recently identified in flies (38), is termed eMI to differentiate it from yeast microautophagy, which is also mediated by microvesicles but independently of ESCRT or hsc70. The current NMR and liposome binding assays pinpoint the lysine cluster (Lys-573, Lys-583, Lys-589, Lys-597, and Lys-601) as the major hsc-70/PS interaction site. Thus, in the next series of experiments the interaction between each of the hsc-70 mutants and late endosomal compartments was analyzed.

Late endosomal compartments were purified by gradient fractionation and labeled with 5-(octadecanoylamino)fluorescein (stearoyl amino fluorescein), a fluorescence lipophilic probe that intercalates with the endosomal limiting membrane and whose fluorescence changes upon lipid/protein interaction (22). The efficiency of endosomal labeling was confirmed by

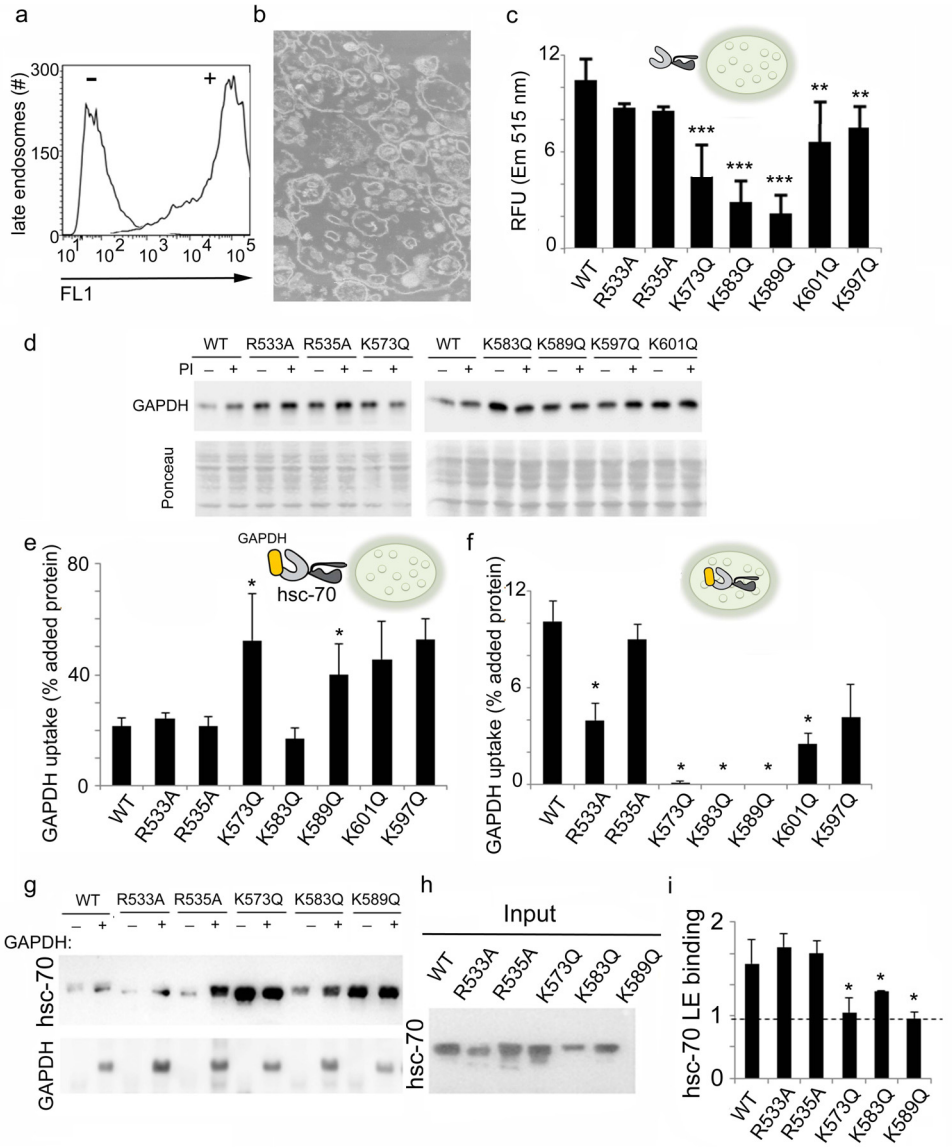

FIGURE 4. **Biological role of hsc-70-PS complex in cytosol-to-endosome protein internalization via endosomal MI.** *a,* FACS analysis of gradient-purified late endosomal compartments plus (+) or minus (−) labeling with (5-(octadecanoylamino) fluorescein) lipophilic probe. *b,* ultrastructural analysis of gradient-purified late endosomes. *c,* late endosomes, fluorescently labeled as in *a,* were incubated with recombinant wild-type hsc-70 or hsc-70 mutants proteins. Changes in fluorescence intensities, indicative of hsc-70 binding to the endosome limiting membrane, are reported as mean and standard deviation. Data were analyzed by one-way ANOVA (**, $p < 0.01$; ***, $p < 0.005$) and Tukey test. *RFU*, relative fluorescence units. *d,* representative immunoblot for GAPDH of endosomes recovered by centrifugation following incubation with GAPDH in the presence of wild type of hsc-70 mutant proteins. Where indicated the protease inhibitors (*PI*) were added to block GAPDH degradation. Ponceau staining is shown at the *bottom* to demonstrate equal endosomal content. *e* and *f,* quantification of the amount of hsc-70-GAPDH bound (*e*) and internalized and degraded (*f*) into endosomes. Internalization and degradation were calculated by discounted GAPDH bound to endosomes in absence of protease inhibitors to that associated with endosomes in the presence of protease inhibitors. Values are expressed as percentage of GAPDH added and are mean and standard deviation ($n = 3$) of the densitometric analysis of immunoblots as the one shown in *d*. Data were analyzed by *t* test (*, $p < 0.05$). *g,* representative immunoblot for hsc-70 (*top*) and GAPDH (*bottom*) of endosomes incubated with wild type of hsc-70 mutants alone (−) or in the presence of GAPDH (+). *h* shows one-fifth of the hsc-70 inputs. *i,* quantification of the amount of hsc-70 bound to endosomes in presence of GAPDH. Values are expressed relative to the amount of hsc-70 bound to endosomes when incubated without GAPDH and are mean and standard deviation ($n = 4$) of the densitometric analysis of immunoblots as the one shown in *g*. Data were analyzed by *t* test (*, $p < 0.05$).

FACS analysis comparing unlabeled *versus* labeled organelles (Fig. 4*a*). The structural integrity of the purified late endosomes was confirmed by transmission electron microscopy (Fig. 4*b*). Labeled endosomes were then incubated with wild-type hsc-70 or hsc-70 mutants, and changes in fluorescence were detected by fluorescence spectroscopy (497 nm excitation and 500–550 nm emission). All mutants presented a decreased lipid-based interaction with the late endosomal limiting membrane similarly to what was previously observed for PS liposomes (Fig. 4*c*).

In the next series of experiments wild-type hsc-70 and each of the mutants were incubated with one of its natural autophagy cargos (the GAPDH protein) in the presence of endosomes untreated or pre-treated with protease inhibitors to analyze the impact of the mutations in cargo binding and internalization, respectively (Fig. 4, *d–f*). Although binding of GAPDH to the surface of endosomes was still observed and even enhanced when incubated in the presence of mutant hsc-70 proteins (Fig. 4, *d* and *e*), we found a significant impairment in the endosomal

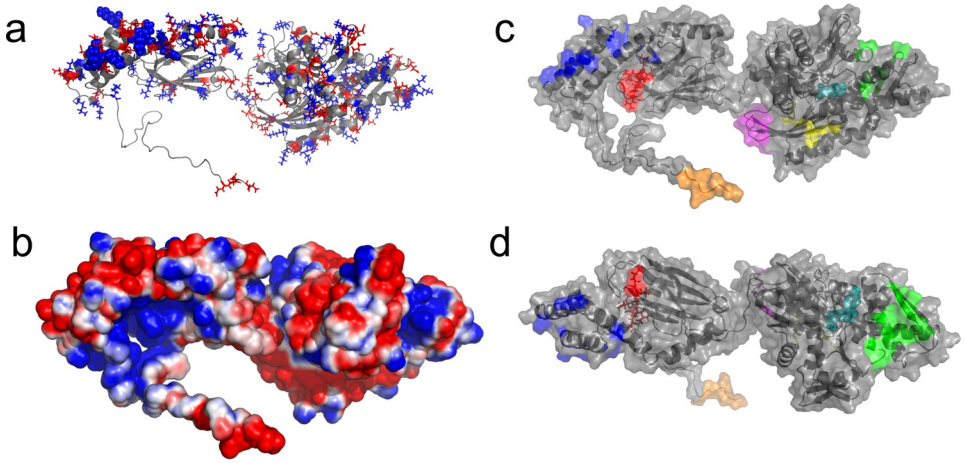

FIGURE 5. **Homology model of wild-type hsc-70.** The model is based on the crystal structures of hsc-70 NBD and hsp-70 (HSPA1) SBD. At *right* is the NBD; at *left* is the SBD. The unstructured peptide at the *left bottom* depicts residues 610–646. *a,* distribution of positive (*blue*) and negative (*red*) residues over hsc-70. The residues Arg-533, Lys-535, Lys-569, Lys-573, Lys-583, Lys-589, Lys-597, and Lys-601 that interact with DOPS and liposomes as defined in this work are shown as *spheres*. *b,* surface electrostatic map in the same orientation as *a*. If a positive/negative charge would touch the *red/blue* surface, it would perceive an attractive energy of 0.6 kcal/mol. *c,* known interaction sites or surfaces of hsc-70. ADP is indicated in *cyan spheres*. The substrate-cleft bound peptide NRLLLTG is shown in *red sticks*. *Blue* is the hsc-70 PS binding area defined in this work. Other binding areas are shown as follows. *Orange*, CHIP-binding site; *magenta*, the HdJ-binding site in analogy to DnaK-DnaJ; *green*, binding site of BAG1; *yellow*, binding site of the MKT077-related hsc-70-modifying compounds. *d,* as *c*, but rotated by 90° along the *horizontal axis*.

internalization of GAPDH, analyzed as the amount of GAPDH degraded in the late endosomal lumen, unless degradation was prevented with protease inhibitors (Fig. 4, *d–f*). To investigate the reasons for the different impact of hsc-70 mutations on cargo binding and internalization, we analyzed binding of hsc-70 to the endosomal membrane in the presence or absence of cargo. As expected from its function in cargo targeting to endosomal microautophagy, the amount of wild-type hsc-70 bound to late endosomes markedly increased upon addition of GAPDH (Fig. 4, *g–i*). In contrast, those mutations that more severely reduced GAPDH internalization still showed an association to the endosomal surface, but it was no longer responsive to the presence of the substrate (Fig. 4, *g–i*). The difference in endosomal binding of these mutants corresponds to the reduction in interaction with the late endosomal limiting membrane (Fig. 4*c*). Overall, these findings confirm the importance of the positively charged residues at the C terminus of the hsc-70 LID for its role in eMI and reveal that the ability of hsc-70 to bind PS is essential at the step of cargo internalization.

Discussion

hsc-70 is a molecular chaperone that plays many important roles in proteostasis and protein trafficking. These activities include at least three fundamentally different functions as follows: (i) a role in protein (re)-folding cycles; (ii) a role in guiding proteins to the proteasome; and (iii) a role in guiding proteins into endosomal/lysosomal compartments for macroautophagy, endosomal microautophagy, and chaperone-mediated autophagy (5–11). hsc-70 carries out each of these activities by interacting with a different set of molecular partners. Although the interaction partners and co-chaperones involved in folding and proteasomal degradation are beginning to be understood (2, 6, 7, 10, 11, 15), the interactions that link hsc-70 to autophagy are much less clear. What is known is that hsc-70 interacts with p62 in the autophagosome to deliver its ubiquitinated cargo through macroautophagy (8), with PS on the endosomal limiting membrane to mediate eMI (21) and that it interacts with lysosomal associate membrane protein type 2A for chaperone-mediated autophagy (8, 21, 22). Still, virtually nothing is known about the structure or biophysics of these interactions.

Although there were previous reports that hsc-70 interacts with membrane PS, the protein itself does not bear any of the canonical protein lipid binding domains. In this study, we set out to delineate and localize the interaction between hsc-70 and PS with a combination of NMR and mutagenesis studies. We carried out two sets of complementary NMR experiments, hsc-70 interaction with DOPS vesicles and with DOPS nanodiscs. As expected for electrostatic interactions, both NMR strategies identified widespread chemical shift perturbations. However, both studies also pointed to larger chemical shift perturbations for the positive residues in the C-terminal tail of the LID. The high density of exposed lysines and arginines in the LID domain appears to be the major site interacting with the negatively charged PS. The C-terminal helix of the LID is not only enriched in positive but also in negative (Glu and Asp) residues (Fig. 5*a*). In fact, the electrostatic potential for this area of the LID is negative rather than positive (Fig. 5*b*). However, these negative residues do not show preferential CSPs as do the positive residues (supplemental Figs. S5 and S6). The specificity of interaction is rather surprising. At the outset, one would expect that an electrostatic interaction with a uniformly negatively charged surface of the artificial DOPS vesicles and nanodiscs would engage virtually every positively charged residue of the protein.

The lack of broadening of the hsc-70 NMR resonances in the presence of the large DOPS discs (100 Å) or vesicles (1000 Å) indicates mobile binding. Indeed, because NMR line widths are inversely proportional to the mobility of the studied molecules, static binding of hsc-70 SBD (with a rotational correlation time (τ_c) of 11 ns) to DOPS vesicles (τ_c of ~1 μs) would have

increased the NMR line width by ~100-fold rendering the NMR spectrum undetectable. We conclude that hsc-70 bound to the vesicles (and the 100 Å nano-discs) remains mobile, likely by being tethered by the long lysine side chains to a fluid-like surface and possibly by diffusing over the uniform DOPS surface.

Specific and systematic chemical shift perturbations were observed for several resonances when the DOPS nano-discs: hsc-70 stoichiometry was increased from 0 to 1.2 with hsc-70 at 44 μM. The occurrence of shifts at these concentration levels indicates that the affinity of the hsc-70 for the DOPS (nano-discs) must be significantly tighter than 50 μM. DOPS nano-discs are uniform in size and ~100 Å in diameter. Therefore, they can in principle accommodate a few hsc-70s on each side of the double layer.

Although we may conclude that the DOPS interaction does occur with the C terminus of the hsc-70 LID domain, we cannot fully exclude interactions with other parts of the protein. However, we have tested by NMR the interaction of DOPS with an isolated nucleotide binding domain of hsc-70(1–386) in the ADP state, and we could not discern any changes in the NMR spectrum (results not shown). Furthermore, although we did not test the hsc-70 dynamically unstructured C-terminal tail (residues 610–646), the electrostatic map (Fig. 5, *a* and *b*) does not show any positive residues or potential for this range, and therefore no interactions with the PS are expected.

By using plasmon resonance (Fig. 1) we estimate an apparent equilibrium dissociation constant of 4.7 ± 0.1 μM for the interaction of WT/hsc-70 with 100% DOPS vesicles, in 100 mM KCl. This number is precise, but not accurate, because binding of a ligand to a surface with a large (and unknown) number of overlapping binding sites is not completely described by the simple binding equation used to calculate the K_D value from the data (23). Nevertheless, from the order of magnitude of the K_D, we may estimate the number of positive hsc-70 residues involved in this interaction. Indeed, Ben-Tal *et al.* (24) determined that synthetic peptides, consisting of 3, 5, or 7 lysine residues to vesicles containing 33% negatively charged phospholipid in 100 mM monovalent salt bind with apparent association constants 5 mM, 180 μM, and 7 μM, respectively. They also determined the dependence of the affinity of penta-lysine as a function of negatively charged phospholipid in the composition range 0–50%. Extrapolating their data to 100%, we predict that 3, 5, or 7 lysine residues would bind to 100% DOPS (in 100 mM salt) with apparent association constants of 300 μM, 2 μM, and 7 nM, respectively. Hence, from our experimental K_D of 4.7 μM, we estimate that a total of 4–5 lysine residues are involved in the interaction with 100% DOPS vesicles.

Previous studies indicate that hsp-70 interacts differently with different lipids and different modalities under physiological or pathological conditions. During stress-induced cell death, hsp-70 stabilizes lysosomes by binding anionic phospholipids such as bis-(monoacylglycero)phosphate (BMP) (25, 26). The authors concluded that the hsp-70 binding to BMP occurs through both its nucleotide binding domain (W-90) and its substrate binding domain (W-580) and suggested that it relies on tryptophan insertion into the lysosomal membrane. However, under physiological conditions W90 is completely buried, and W580 is partially buried in the hsc-70 or hsp-70 core (*versus* PDB codes 3HSC and 4PO2) and is unavailable for insertion. It should be noted that hsp-70 binding to BMP is pH-dependent (25, 26). Possibly, the low pH exposes the tryptophan for insertion into the lipid bilayer (25, 26).

In contrast, both hsc-70 and hsp-70 have also been reported to bind other lipids such as PS. This binding did not require insertion into the PS-containing membrane and was mediated by the substrate-binding LID domain (25, 26).

The NMR measurements and mutagenesis studies presented herein point to the involvement of positively charged residues in the hsc-70 C-terminal LID section for the interaction with negatively charged lipids. As can be seen in Fig. 2, *d* and *h*, where the results of the NMR and mutagenesis studies are both visualized on a model of hsc-70 SBD, the correlation is good but not perfect. Several factors can contribute to this partial mismatch. The first and most simple factor is that mutant K569Q was not sufficiently expressed to test the protein for the site with the largest NMR CSP (Fig. 2*g*). Second, the lysine and arginine NMR CSPs, which report on the chemical environment of the backbone amide groups, likely under-report chemical environmental changes occurring at the peripherally charged groups of these residues. Conversely, an electrostatic field such as that emanating from the DOPS entities may cause shifts on residues that are not truly interacting with those entities. Last and not least, interactions at one site may cause CSPs elsewhere due to conformational changes. Despite all these shortcomings, the fact remains that the NMR CSPs are the largest for some of the lysine side chains that are also implied by mutagenesis.

Other proteins have been shown to use electrostatic interaction surfaces to bind lipid (17). Indeed, this amphiphilic (cationic/hydrophobic) strategy is used by several biological structures to insert into anionic membranes, especially those containing PS. Although PS is present in all cellular membranes, it only confers a negative charge to the plasma and the endosomal membranes; PS present in mitochondria, Golgi, and endoplasmic reticulum is confined to their luminal leaflets and therefore does not charge their cytosolic interfaces (17). It has also been shown that PS directs proteins with strong positive charge to the cytosolic leaflet of the plasma membrane and proteins with moderate positive charge to the cytosolic leaflet of the endosomal membrane (17).

It is tempting to speculate on the structural origin of the lack of DOPS interaction with hsc-70 in the ATP state (Fig. 1, *d* and *e*). Although no structure is known for hsc-70 in this state, it is known for the *E. coli* homologue DnaK that the LID domain is swept away from the SBD and docked to the NBD (27, 28). Could this be the cause of the ATP-dependent change in DOPS interaction in hsc-70? Regretfully, homology between DnaK and hsc-70 in the LID domain is non-existent beyond residue 584, where we find many interactions with DOPS. This area contains no positively charged residues in DnaK. Hence, the LID docking in the DnaK crystal structures would likely not pertain to hsc-70. Nevertheless, LID docking in hsc-70 could explain the difference in nucleotide-dependent PS binding.

hsc-70 is a hub in cellular proteostasis. The protein interacts with many different molecules, substrates, nucleotides,

co-chaperones, and allosteric effectors. Most remarkable is that the protein uses different surfaces for all interactions mapped to date (Fig. 5, *c* and *d*). Nucleotides (ATP and ADP) bind into a deep pocket in the NBD (29); hydrophobic substrates (unfolded proteins) bind to a hydrophobic cleft in the SBD that is guarded by the LID (30). J-proteins (such as DnaJA1 and DnaJB4) affect the interaction between the NBD and SBD by locating into the area between them (19, 31); nucleotide exchange factors of the BAG family (BAG 1, 3, and 6) interact with tips of the NBD domain lobes (32, 33); the E3-ubiquitin ligase CHIP interacts with the very C terminus (15). Potent synthetic regulators derived from the rhodamine MKT077 interact with a conserved site close to the nucleotide-binding site in hsc-70 (34, 35). Other synthetic compounds occupy yet other sites on this protein or its bacterial homologue (36, 37). The herein delineated endosome interaction surface is at another location again. Our studies reveal a unique surface required for the interaction of hsc-70 with late endosomes that is essential for its role in endosomal microautophagy.

Endosomal microautophagy is an ESCRT-dependent process, which is different from the ESCRT-dependent transport of ubiquitinated plasma membrane proteins into the endosomes, and relies on the cytosolic chaperone hsc-70 for the endosomal internalization of cytosolic proteins (8, 38, 39). Although hsc-70 can bind misfolded and ubiquitinated proteins, we previously demonstrated that in endosomal microautophagy, hsc-70 also binds proteins with KFERQ motifs. Thus, although the endosomal vesiculation, *per se*, is ESCRT-dependent, cargo internalization into the endosomes involves different chaperones and/or molecular partners when the cargo is membrane-bound or soluble and when it is ubiquitinated or not. The ESCRT-dependent process described in this work is an autophagic process, because it mediates degradation of intracellular proteins inside endo/lysosomes, whereas the ESCRT-mediated degradation of plasma membrane proteins by the endo/lysosomal system has been correctly classified as an endocytic process. We use the term "microautophagy" to differentiate from other cellular forms of autophagy, such as macroautophagy or chaperone-mediated autophagy, and to highlight the morphological similarity of this process to microautophagy described in yeast. However, because the equivalent to the vacuolar yeast in mammals would be lysosomes and this process of autophagy mediated by hsc-70 and ESCRT occurs in endosomes and not in lysosomes, it is necessary to include the term "endosomal" to clarify the compartment where this type of autophagy takes place.

Our work with mutant hsc-70 and isolated endosomes reveals that the positively charged region of the hsc-70-LID is not required for substrate binding to late endosomes but it is absolutely necessary for substrate internalization. Because our structural data and analysis in liposomes reveal that this is the region utilized by hsc-70 to bind PS, it is possible that binding of hsc-70 to PS is the trigger for microvesicle formation and that the latter only forms at membrane micro-domains enriched in PS. Whether hsc-70 binding to PS is directly responsible for the recently described membrane deforming activity of this chaperone (38) requires future investigation.

Importantly, the hsc-70/PS interaction occurring under physiological conditions only requires a 'lateral" interaction with the late endosomal compartments, without protein embedding into the lipid bilayer. Such interaction would facilitate the entry of the hsc-70/cargo into the forming vesicles. In contrast, this interaction is different from what is observed during pathological conditions when lysosomal membrane destabilization requires hsc-70 embedding into the organelle-limiting membrane to preserve endosomal integrity (25, 26).

Altogether, our data add an additional piece to the puzzle of hsc-70 multivalent interactions. Considering the pivotal role of this protein in cellular proteostasis, there has been considerable interest in generating small molecules and peptides acting as hsc-70 modulators. Our data, providing a novel site for hsc-70 interaction with PS membrane, could provide a novel site for the development of therapeutical hsc-70 modulators.

Experimental Procedures

Preparation of Liposomes—1,2-Dioleoyl-*sn*-glycero-3-phospho-L-serine (DOPS) (catalog no. 840035C), 1,2-dioleoyl-*sn*-glycero-3-phosphocholine (DOPC) (catalog no. 850375C), and cholesterol (catalog no. 700000P) were purchased from Avanti Polar Lipids (Alabaster, AL). Chloroform solutions of DOPS, DOPC, and cholesterol were lyophilized on a rotary evaporator overnight. Lipid films were re-hydrated with 0.9% NaCl solution followed by sonication and extrusion through a polycarbonate membrane with a pore size of 0.05 μm using a Mini-Extruder (Avanti Polar Lipids). Three types of unilamellar liposomes were obtained, DOPS, DOPC, and DOPC/cholesterol, which were gassed with argon stream and stored overnight at 4 °C prior to binding assays. To check the quality of liposomal preparation, 10 μl of each liposome solution were spotted on Formvar-coated grids, stained with 1% phosphotungstic acid and viewed, with a Jeol JEM-1200EX transmission electron microscope at 80 kV.

Liposome Binding Assay—For binding experiments, 5 μg of recombinant hsc-70 (full-length wild type and mutants) were incubated with DOPS, DOPC, and DOPC/cholesterol liposomes for 30 min at 37 °C in the presence or absence of 20 mM ATP. Binding was analyzed via Western blotting following the separation of liposome-bound and -unbound hsc-70 by ultracentrifugation at 35,000 rpm for 1 h at 4 °C.

hsc-70 Mutagenesis—The hsc-70 mutants (R533A, R535A, K573Q, K583Q, K589Q, K597Q, and K601Q) were generated using site-directed mutagenesis with the mouse wild-type hsc-70 cDNA as template (GenScript, Piscataway, NJ). The following primers were used: R533A forward, 5′-AGGATGAGAAGCAGGCCGATAAGGTTTCCTCCAAGAAC3-′, and reverse, 5′-GGAAACCTTATCGGCCTGCTTCTCATCCTCAGCCTT-3′; R535A forward, 5′-AGAAGCAGAGAGATGCCGTTTCCTCCAAGAACTCACTGG-3′, and reverse, 5′-TCTTGGAGGAAACGGCATCTCTCTGCTTCTCATCC-3′; K573Q forward, 5′-CACAGAAGATTCTTGACCAGTGCAATGAAATCATC-3′, and reverse, 5′-GATGATTTCATTGCACTGGTCAAGAATCTTCTGTG-3′; K583Q forward, 5′-GAAATCATCAGCTGGCTGGATCAGAACCAGACTGCAGAGAAGG-3′, and reverse, 5′-CCTTCTCTGCAGTCTGGTTCTGATCCAGCCAGCTGATGATTTC-3′; K589Q forward,

5′-GAACCAGACTGCAGAGCAGGAAGAATTTGAGC-3′, and reverse, 5′-GCTCAAATTCTTCCTGCTCTGCAGTCT-GGTTC-3′; K597Q forward, 5′-GAATTTGAGCATCAGCA-GCAAGAACTGGAGAAAGTC-3′, and reverse, 5′-GACTT-TCTCCAGTTCTTGCTGCTGATGCTCAAATTC-3′; K601Q forward, 5′-GCAGAAAGAACTGGAGCAAGTCTGCAACC-CTATC-3′, and reverse, 5′-GATAGGGTTGCAGACTT-GCTCCAGTTCTTTCTGC-3′.

Production of Recombinant hsc-70—Wild-type hsc-70 and mutant proteins were inserted into pTrcHis B or pTrcHis A (for truncated) vectors. Protein production was induced with 1 mM isopropyl 1-thio-β-D-galactopyranoside for 12 h, and all proteins were purified from the bacterial lysates using a Ni^{2+}-charged His-Bind resin column (Novagen, EMD Chemicals, Gibson, NJ) by FPLC purification. Protein expression and purity were assessed by SDS-PAGE followed by silver staining.

Late Endosome Preparation—Mouse dendritic cells (JAWS) were maintained in Dulbecco's modified Eagle's medium (DMEM) (Sigma), in the presence of 10% fetal bovine serum (FBS), 50 μg/ml penicillin, and 50 μg/ml streptomycin at 37 °C with 5% CO_2 and tested for mycoplasma contamination every 2 weeks using a DNA staining protocol with Hoechst 33258 dye or MycoSensor PCR assay kit (Stratagene). Cells ($1–3 \times 10^8$) were pelleted, washed in PBS, and resuspended in PBS containing 0.25 M sucrose and 20 mM HEPES, pH 7.4. LE and lysosomes were isolated as reported previously (8). Briefly, cells were homogenized in a Dounce homogenizer and spun at 3,100 rpm for 10 min. The supernatant was loaded on a 27% Percoll gradient laid over a 2.5 M sucrose cushion and centrifuged for 1 h at 14,000 rpm. The band above the sucrose cushion corresponds to the total lysosomal fraction. The band at the interface was enriched in late and early endosomes and was further separated on a 10% Percoll gradient by centrifugation at 14,000 rpm for 1 h. The purity of the LE fraction was confirmed by ultrastructural analysis and Western blotting for selected markers (8). In addition, the purity of the LE fraction was confirmed by the levels of β-hexosaminidase, using a sodium acetate buffer, pH 4.0, and 4-methylumbelliferyl-*N*-acetyl-β-D-glucosaminide as substrate (8).

Labeling of LE with Fluorescent Probe and LE Binding Assay—hsc-70 binding to highly purified late endosomes was performed using a fluorescence probe (5-(octadecanoylamino) fluorescein) (stearoyl amino fluorescein) (MGT Inc.) that is sensitive to the physical and chemical integrity as well as lipid composition of the organelle's limiting membrane using the procedure already described in detail elsewhere (8). Briefly, 10 μg of LE were incubated with 0.5 μg of the fluorescein-based probe, previously optimized to give a signal/noise of >3 as compared with the probe itself. Endosomal fluorescence was confirmed by FACS analysis. Binding of each wild type and hsc-70 mutants (15 μg/each protein) to a purified and fluorescently labeled LE fraction was monitored by fluorescence spectroscopy (497 nm excitation, 500–550 nm emission; 5.0-nm slit width and 0.5-s response time). The change in fluorescence at 520 nm (maximum emission) due to hsc-70 binding to LE was plotted as relative fluorescence units. The statistical significance for the differential binding of wild-type and mutant hsc-70 to LE was evaluated with the two-tailed unpaired one-way ANOVA. A p value <0.05 was evaluated as statistically significant.

Surface Plasmon Resonance—All surface plasmon resonance experiments were performed on a BIAcore 3000, using L1 sensor chips. Large unilamellar vesicles were first prepared by evaporating either 1-palmitoyl-2-oleoyl-*sn*-glycero-3-phosphocholine or 1-palmitoyl-2-oleoyl-*sn*-glycerol-3-phosphoserine (Avanti) from chloroform under a nitrogen stream. Evaporated lipids were then resuspended in buffer and vortexed prior to extrusion 20–30 times using 100-nm filters. Extruded vesicles were loaded onto L1 chips and washed with degassed buffer (10 mM HEPES, pH 7.2, 100 mM NaCl) to a final loading density of ~5000 RU. Hsc70 in running buffer was injected (10 μl/min flow rate), and binding was monitored in BiaEval software. Fitting of the equilibrium values (750 s) was performed in GraphPad PRISM.

Statistical Analysis—All numerical results are reported as mean ± S.E., and represent data from a minimum of three independent experiments unless otherwise stated. In all instances, n refers to individual experiments. A p value <0.05 was evaluated as statistically significant. Statistical analysis was performed using Windows GraphPad Prism 6 (GraphPad Software, La Jolla, CA). Comparisons of the hsc-70 binding to the fluorescent-labeled LE between wild type and each mutant protein were performed using the two-tailed unpaired one-way ANOVA.

Measurement of Endosomal Activity—e-MI activity *in vitro* was measured using rat liver isolated late endosomes incubated with purified proteins and subjected to immunoblot (8). Adult (4 months of age) male Wistar rats were from Charles River Laboratories and were used under an institution-approved animal study protocol. All animals (<3 rats per cage) were maintained in 12-h light/dark cycles. Endosomes were isolated as described previously (8), and binding and internalization were calculated as the amount of substrate protein bound to the late endosomal membrane and intact internal vesicles in the absence of protease inhibitors and luminal degradation by subtracting the amount of protein associated with late endosomes in the presence (protein bound to the endosomal membrane, intact internal vesicles, and inside late endosomal lumen) and absence (protein bound to the endosomal membrane and intact internal vesicles) of protease inhibitors.

hsc-70 PS NMR—The NMR experiments for DOPS vesicle binding were carried out with ^{15}N-labeled hsc-70(395–604) bound to the TAU peptide KVQIINKKGCGMGHHHHHH. The data were collected on a 900 MHz Bruker NMR spectrometer equipped with a triple-resonance cold probe using 54 mM hsc-70(395–604) in 50 mM Tris, 100 mM KCl, 10 mM KP_i, pH 7.2, 5% HOD. Different amounts of 10 mM DOPS solution in the same buffer were added. The aqueous DOPS solution was prepared by evaporating the solvent from DOPS in chloroform prior to adding buffer. DOPS was purchased from Avanti Polar Lipids, Inc. (Alabaster, AL).

Four ^{15}N-^{1}H TROSY experiments (10 h each) were collected at 30 °C all with SBD at 54 mM, τ at 165 mM, and DOPS at 0, 33, 165, and 1650 mM, respectively. The data were processed in NMRPipe, and overlaid and plotted in Sparky.

The NMR experiments for binding DOPS nano-discs were carried out with ^{15}N-labeled hsc-70(395–604) bound to the peptide MHHHHHHSSGVDLGTENLYFQSNA. The data were collected on a 600 MHz Bruker NMR spectrometer equipped with a triple-resonance cold probe. A sample of 250 μl of 80 mM hsc-70(395–604) in 50 mM Tris, 100 mM KCl, 10 mM KP_i, pH 7.2, 5% HOD, was titrated with 200 ml of DOPS nano-discs, at 125 mM. The nano-disc protein, MSP1D1ΔH5, was purchased from Cube Biotech (Mannheim, Germany), and the discs were prepared by adapting the generic protocol to DOPS (19). Excess lipids were removed from the nano-disc solution by G25 gel filtration.

Three ^{15}N-^{1}H TROSY experiments were collected at 30 °C as follows: 1) hsc-70 at 80 mM without DOPS (2 h); 2) hsc-70 at 57 mM, DOPS discs at 36 mM (6 h); and 3) hsc-70 at 44 mM, DOPS discs at 55 mM (9 h). The data were processed in NMRPipe, and overlaid and plotted in Sparky. The NMR peak assignments were obtained from 800 MHz triple-resonance data (TROSY forms of HNCA, HNCOCA, HNCO, HNCACO, and HNCACB) obtained on an identical hsc-70 SBD construct, using the program EZ-ASSIGN.

The homology model for human hsc-70 SBD bound to NRLLLTG was constructed from the crystal structure coordinates for human hsp-70(386–613) (PDB code 4PO2). Amino acid replacements to obtain the hsc-70 sequence were made in PyMOL, and the model was relaxed with AMBER.

The homology model for full-length hsc-70 started with the SBD homology model. Amino acids 614–646 were added in PyMOL. The coordinates for the NBD were from PDB code 3HSC (ADP-bound). The relative orientations and locations of NBD and SBD were modeled after *E. coli* DnaK (PDB code 2KHO). NBD-SBD linker residues were constructed in PyMOL and AMBER. The model was relaxed with AMBER molecular dynamics runs.

Author Contributions—J. E. G., A. M. C., E. R. P. Z., and L. S. designed the experiments; E. R. P. Z., K. M., C. C. C., S. K., B. S., E. A., A. A., J. N. R., V. C., C. M., and B. S. performed the experiments; K. M., J. E. G., A. M. C., E. R. P. Z., and L. S. wrote the paper.

References

1. Kampinga, H. H., Hageman, J., Vos, M. J., Kubota, H., Tanguay, R. M., Bruford, E. A., Cheetham, M. E., Chen, B., and Hightower, L. E. (2009) Guidelines for the nomenclature of the human heat shock proteins. *Cell Stress Chaperones* **14,** 105–111
2. Zuiderweg, E. R., Bertelsen, E. B., Rousaki, A., Mayer, M. P., Gestwicki, J. E., and Ahmad, A. (2013) Allostery in the Hsp70 chaperone proteins. *Top. Curr. Chem.* **328,** 99–153
3. McCarty, J. S., Buchberger, A., Reinstein, J., and Bukau, B. (1995) The role of ATP in the functional cycle of the DnaK chaperone system. *J. Mol. Biol.* **249,** 126–137
4. Szabo, A., Langer, T., Schröder, H., Flanagan, J., Bukau, B., and Hartl, F. U. (1994) The ATP hydrolysis-dependent reaction cycle of the *Escherichia coli* Hsp70 system DnaK, DnaJ, and GrpE. *Proc. Natl. Acad. Sci. U.S.A.* **91,** 10345–10349
5. Schröder, H., Langer, T., Hartl, F. U., and Bukau, B. (1993) DnaK, DnaJ and GrpE form a cellular chaperone machinery capable of repairing heat-induced protein damage. *EMBO J.* **12,** 4137–4144
6. Jiang, J., Ballinger, C. A., Wu, Y., Dai, Q., Cyr, D. M., Höhfeld, J., and Patterson, C. (2001) CHIP is a U-box-dependent E3 ubiquitin ligase: identification of Hsc70 as a target for ubiquitylation. *J. Biol. Chem.* **276,** 42938–42944
7. Lüders, J., Demand, J., and Höhfeld, J. (2000) The ubiquitin-related BAG-1 provides a link between the molecular chaperones Hsc70/Hsp70 and the proteasome. *J. Biol. Chem.* **275,** 4613–4617
8. Sahu, R., Kaushik, S., Clement, C. C., Cannizzo, E. S., Scharf, B., Follenzi, A., Potolicchio, I., Nieves, E., Cuervo, A. M., and Santambrogio, L. (2011) Microautophagy of cytosolic proteins by late endosomes. *Dev. Cell* **20,** 131–139
9. Orenstein, S. J., and Cuervo, A. M. (2010) Chaperone-mediated autophagy: molecular mechanisms and physiological relevance. *Semin. Cell Dev. Biol.* **21,** 719–726
10. Gamerdinger, M., Kaya, A. M., Wolfrum, U., Clement, A. M., and Behl, C. (2011) BAG3 mediates chaperone-based aggresome-targeting and selective autophagy of misfolded proteins. *EMBO Rep.* **12,** 149–156
11. Arndt, V., Rogon, C., and Höhfeld, J. (2007) To be, or not to be–molecular chaperones in protein degradation. *Cell. Mol. Life Sci.* **64,** 2525–2541
12. Garimella, R., Liu, X., Qiao, W., Liang, X., Zuiderweg, E. R., Riley, M. I., and Van Doren, S. R. (2006) Hsc70 contacts helix III of the J domain from polyomavirus T antigens: addressing a dilemma in the chaperone hypothesis of how they release E2F from pRb. *Biochemistry* **45,** 6917–6929
13. Morshauser, R. C., Hu, W., Wang, H., Pang, Y., Flynn, G. C., and Zuiderweg, E. R. (1999) High-resolution solution structure of the 18-kDa substrate binding domain of the mammalian chaperone protein Hsc70. *J. Mol. Biol.* **289,** 1387–1403
14. Morshauser, R. C., Wang, H., Flynn, G. C., and Zuiderweg, E. R. (1995) The peptide binding domain of the chaperone protein Hsc70 has an unusual secondary structure topology. *Biochemistry* **34,** 6261–6266
15. Smith, M. C., Scaglione, K. M., Assimon, V. A., Patury, S., Thompson, A. D., Dickey, C. A., Southworth, D. R., Paulson, H. L., Gestwicki, J. E., and Zuiderweg, E. R. (2013) The E3 ubiquitin ligase CHIP and the molecular chaperone Hsc70 form a dynamic, tethered complex. *Biochemistry* **52,** 5354–5364
16. Arispe, N., and De Maio, A. (2000) ATP and ADP modulate a cation channel formed by Hsc70 in acidic phospholipid membranes. *J. Biol. Chem.* **275,** 30839–30843
17. Yeung, T., Gilbert, G. E., Shi, J., Silvius, J., Kapus, A., and Grinstein, S. (2008) Membrane phosphatidylserine regulates surface charge and protein localization. *Science* **319,** 210–213
18. Bayburt, T. H., and Sligar, S. G. (2003) Self-assembly of single integral membrane proteins into soluble nanoscale phospholipid bilayers. *Protein Sci.* **12,** 2476–2481
19. Ahmad, A., Bhattacharya, A., McDonald, R. A., Cordes, M., Ellington, B., Bertelsen, E. B., and Zuiderweg, E. R. (2011) Heat shock protein 70-kDa chaperone/DnaJ cochaperone complex employs an unusual dynamic interface. *Proc. Natl. Acad. Sci. U.S.A.* **108,** 18966–18971
20. Guan, J. Y., Foerster, J. M., Drijfhout, J. W., Timmer, M., Blok, A., Ullmann, G. M., and Ubbink, M. (2014) An ensemble of rapidly interconverting orientations in electrostatic protein-peptide complexes characterized by NMR spectroscopy. *Chembiochem* **15,** 556–566
21. Iwahara, J., and Clore, G. M. (2006) Detecting transient intermediates in macromolecular binding by paramagnetic NMR. *Nature* **440,** 1227–1230
22. Horobin, R. W. (2002) Biological staining: mechanisms and theory. *Biotech. Histochem.* **77,** 3–13
23. Heimburg, T., and Biltonen, R. L. (1996) A Monte Carlo simulation study of protein-induced heat capacity changes and lipid-induced protein clustering. *Biophys. J.* **70,** 84–96
24. Ben-Tal, N., Ben-Shaul, A., Nicholls, A., and Honig, B. (1996) Free-energy determinants of α-helix insertion into lipid bilayers. *Biophys. J.* **70,** 1803–1812
25. Kirkegaard, T., Roth, A. G., Petersen, N. H., Mahalka, A. K., Olsen, O. D., Moilanen, I., Zylicz, A., Knudsen, J., Sandhoff, K., Arenz, C., Kinnunen, P. K., Nylandsted, J., and Jäättelä, M. (2010) Hsp70 stabilizes lysosomes and reverts Niemann-Pick disease-associated lysosomal pathology. *Nature* **463,** 549–553
26. Mahalka, A. K., Kirkegaard, T., Jukola, L. T., Jäättelä, M., and Kinnunen, P. K. (2014) Human heat shock protein 70 (Hsp70) as a peripheral membrane protein. *Biochim. Biophys. Acta* **1838,** 1344–1361

27. Qi, R., Sarbeng, E. B., Liu, Q., Le, K. Q., Xu, X., Xu, H., Yang, J., Wong, J. L., Vorvis, C., Hendrickson, W. A., Zhou, L., and Liu, Q. (2013) Allosteric opening of the polypeptide-binding site when an Hsp70 binds ATP. *Nat. Struct. Mol. Biol.* **20,** 900–907
28. Kityk, R., Kopp, J., Sinning, I., and Mayer, M. P. (2012) Structure and dynamics of the ATP-bound open conformation of Hsp70 chaperones. *Mol. Cell* **48,** 863–874
29. Flaherty, K. M., DeLuca-Flaherty, C., and McKay, D. B. (1990) Three-dimensional structure of the ATPase fragment of a 70K heat-shock cognate protein. *Nature* **346,** 623–628
30. Zhu, X., Zhao, X., Burkholder, W. F., Gragerov, A., Ogata, C. M., Gottesman, M. E., and Hendrickson, W. A. (1996) Structural analysis of substrate binding by the molecular chaperone DnaK. *Science* **272,** 1606–1614
31. Suh, W. C., Lu, C. Z., and Gross, C. A. (1999) Structural features required for the interaction of the Hsp70 molecular chaperone DnaK with its co-chaperone DnaJ. *J. Biol. Chem.* **274,** 30534–30539
32. Sondermann, H., Scheufler, C., Schneider, C., Hohfeld, J., Hartl, F. U., and Moarefi, I. (2001) Structure of a Bag/Hsc70 complex: convergent functional evolution of Hsp70 nucleotide exchange factors. *Science* **291,** 1553–1557
33. Kabbage, M., and Dickman, M. B. (2008) The BAG proteins: a ubiquitous family of chaperone regulators. *Cell. Mol. Life Sci.* **65,** 1390–1402
34. Rousaki, A., Miyata, Y., Jinwal, U. K., Dickey, C. A., Gestwicki, J. E., and Zuiderweg, E. R. (2011) Allosteric drugs: the interaction of antitumor compound MKT-077 with human Hsp70 chaperones. *J. Mol. Biol.* **411,** 614–632
35. Li, X., Srinivasan, S. R., Connarn, J., Ahmad, A., Young, Z. T., Kabza, A. M., Zuiderweg, E. R., Sun, D., and Gestwicki, J. E. (2013) Analogs of the allosteric heat shock protein 70 (Hsp70) inhibitor, MKT-077, as anti-cancer agents. *ACS Med. Chem. Lett.* **4,** 10.1021/ml400204n
36. Leu, J. I., Zhang, P., Murphy, M. E., Marmorstein, R., and George, D. L. (2014) Structural basis for the inhibition of HSP70 and DnaK chaperones by small-molecule targeting of a C-terminal allosteric pocket. *ACS Chem. Biol.* **9,** 2508–2516
37. Chang, L., Miyata, Y., Ung, P. M., Bertelsen, E. B., McQuade, T. J., Carlson, H. A., Zuiderweg, E. R., and Gestwicki, J. E. (2011) Chemical screens against a reconstituted multiprotein complex: myricetin blocks DnaJ regulation of DnaK through an allosteric mechanism. *Chem. Biol.* **18,** 210–221
38. Uytterhoeven, V., Lauwers, E., Maes, I., Miskiewicz, K., Melo, M. N., Swerts, J., Kuenen, S., Wittocx, R., Corthout, N., Marrink, S. J., Munck, S., and Verstreken, P. (2015) Hsc70–4 deforms membranes to promote synaptic protein turnover by endosomal microautophagy. *Neuron* **88,** 735–748
39. Mukherjee, A., Koga, H., Patel, B., Cuervo, A.M., Jenny, A. (2016) Selective endosomal microphage starvation inducible in *Drosophila*. *Autophagy*